# Long-Lived Polaritonic Coherence and Polaron Decoupling Effects in 2D Electronic Spectra

M. Elious Mondal,[1, a)] Seongje Park,[2, 3] Minjung Son,[2, 3] A. Nickolas Vamivakas,[4, 5, 6] Steven T. Cundiff,[7] Todd D. Krauss,[1, 4, 6] and Pengfei Huo[1, 4, 6, b)]

[1)] *Department of Chemistry, University of Rochester, Rochester, New York, 14627, USA*

[2)] *Department of Chemistry, Boston University, Boston, Massachusetts, 02215, USA*

[3)] *Boston University Photonics Center, Boston, Massachusetts, 02215, USA*

[4)] *The Institute of Optics, Hajim School of Engineering, University of Rochester, Rochester, NY 14627, USA*

[5)] *Department of Physics and Astronomy, University of Rochester, Rochester, NY 14627, USA*

[6)] *Center for Coherence and Quantum Optics, University of Rochester, Rochester, New York 14627, USA*

[7)] *Department of Physics, University of Michigan, Ann Arbor, MI 48109, USA*

(Dated: 21 October 2025)

Molecular polaritons, the hybridization of excitonic states in molecules with photonic excitation inside a cavity, play an important role in fundamental quantum science and technology. Understanding the decoherence mechanism of molecular polaritons is among the most significant fundamental questions. We theoretically demonstrate that hybridizing many molecular excitons in a cavity protects the overall quantum coherence from phonon-induced decoherence. The polariton coherence time can be prolonged up to 200 fs with a realistic collective Rabi splitting and quality factor at room temperature, compared to the typical electronic coherence time, which is around 15 fs. We directly simulate 2D electronic spectra (2DES) and demonstrate a prolonged oscillation period of the off-diagonal beating between the upper polariton and lower polariton state. Our simulations demonstrate that the nodal line slope (NLS) of the lower polariton diagonal peak decreases, indicating the decoupling from vibrations. These direct simulations of the prolonged polariton coherence will provide invaluable guidance for our ongoing experimental verification of coupling CdSe nanoplatelets to the optical cavity.

## I. INTRODUCTION

Coupling molecules to a quantized radiation field inside an optical cavity produces a set of photon-matter hybrid (entangled) states known as polaritons. These polariton states, which are hybridizations of the excitons and photons, have been shown to possess the properties of both and have enabled novel many-body physics, new chemical reactivities[1], and new spectroscopic signals[2–6]. In particular, recent theoretical and experimental work has suggested that due to the collective light-matter coupling, the polariton states are effectively decoupled from the molecular vibrations, which is referred to as the polaron decoupling effect. This effect originates from the effective reduction of the vibrational reorganization energy $\lambda$ when increasing the collective coupling between light and matter, characterized by $\Omega_{\mathrm{R}} = 2\sqrt{N}g_{\mathrm{c}}$, where $N$ is the number of molecules and $g_{\mathrm{c}}$ is the coupling strength between the cavity mode per molecule. Theoretical analysis[7–11] suggests that $\lambda$ will decrease with a scaling of $1/N$. The polaron decoupling effect has been experimentally verified by linear spectra,[3,4,12], as well as non-linear 2DES spectra[2]. Due to the effective polaron decoupling effect, it is possible to achieve a long-lived polaritonic coherence even at room temperature. Indeed, our preliminary theoretical work[9] suggests that it is possible to prolong the exciton coherence from the original 15 fs to exciton-polariton coherence up to 200 fs in a model system with parameters that describes CdSe Nanoplatelet coupled to an optical cavity[13–16], with the explicit consideration of both cavity loss and decay to the dark states[9,17]. However, a direct theoretical simulation that verifies such prolonged coherence in 2DES remains missing due to both the computational challenge to accurately simulate 2DES spectra while taking care of the non-Markovian behavior of the phonon dynamics, explicitly considering the cavity loss, as well as the unfavorable scaling to simulate the model system under the collective light-matter couplings. To address this challenge, we have developed state-of-the-art theoretical approaches[17–19] that use stochastic Lindblad dynamics[17,20] to model the cavity loss effect and the partially linearized path-integral approach[21–24] to simulate exciton polariton dynamics coupled to the phonon vibrations. We developed quantum dynamics propagation algorithms[17] leveraging the symmetry of collective light-matter interactions to efficiently simulate polariton 2DES[18,19]. These methods enable the first-time simulation of time-dependent 2DES, revealing prolonged off-diagonal beating between the upper and lower polariton states, which aligns with polaron decoupling effects also indicated by the flattening of nodal line slope (NLS) of diagonal peaks in pure-absorptive 2DES.

[a)] Electronic mail: mmondal@ur.rochester.edu

[b)] Electronic mail: pengfei.huo@rochester.edu

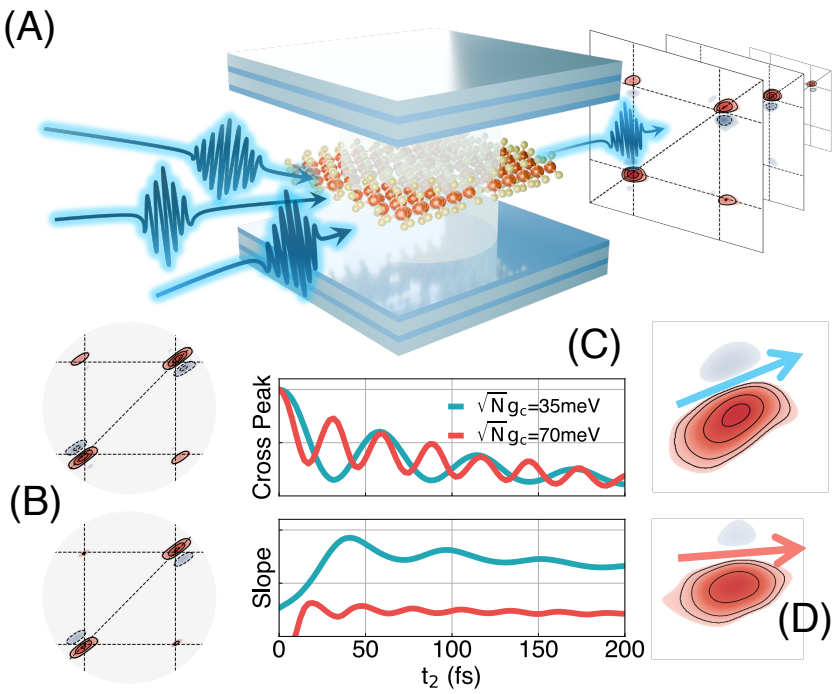


FIG. 1. **Schematic illustration of the collective light-matter coupling, the polaron decoupling effect, and its consequences in non-linear spectra.** (A) Schematic illustration of a 2DES setup on a polaritonic sample of CdSe Nanoplatelet coupled to an FP cavity. (B) The rephasing 2DES signal at two different $t_2$ to demonstrate the beating of off-diagonal cross peak (C) The cross-peak and NLS behaviour at different values of $\sqrt{N}g_c$, (D) The lower diagonal 2DES peak (LP diagonal peak) with $\sqrt{N}g_c$=35 meV and $\sqrt{N}g_c$=70 meV, and a cavity quality factor $\mathcal{Q} = 10$ meV.

## II. THEORETICAL MODEL

We use the Holstein-Tavis-Cummings Hamiltonian[13,18,25] to describe $N$-molecules collectively coupled to a single cavity mode as follows

$$\hat{H} = \sum_{n=1}^{N} \varepsilon_n \hat{\sigma}_n^\dagger \hat{\sigma}_n + \hat{H}_{\rm sb} + \hat{H}_{\rm b} + \hbar\omega_{\rm c}\Big(\hat{a}^\dagger\hat{a} + \frac{1}{2}\Big) + \sum_{n=1}^{N} \hbar g_{\rm c}\left(\hat{\sigma}_n^\dagger \hat{a} + \hat{\sigma}_n \hat{a}^\dagger\right) \tag{1}$$

where the $n_{\rm th}$ exciton has site energy of $\varepsilon_n$ and the exciton is coupled to the cavity mode of energy $\omega_{\rm c}$ with a light-matter coupling strength of $g_{\rm c}$. Here, $\hat{\sigma}_n^\dagger = |e_n\rangle\langle g_n|$ and $\hat{\sigma}_n = |g_n\rangle\langle e_n|$ create and annihilate an excitation on the $n_{\rm th}$ molecule, respectively, with $|g_n\rangle$ and $|e_n\rangle$ as the ground and excited states for molecule $n$. Further, each exciton state is coupled to a set of independent phonon baths, described by $\hat{H}_{\rm b} = \sum_{n=1}^{N}\sum_{\nu}(\hat{b}_{n,\nu}^\dagger \hat{b}_{n,\nu} + \frac{1}{2})$ where $\hat{b}_{n,\nu}^\dagger$ and $\hat{b}_{n,\nu}$ are the creation and annihilation operators of the $\nu_{\rm th}$ phonon. The phonon is coupled to the $n_{\rm th}$ exciton through $\hat{H}_{\rm sb} = \sum_n \hat{\sigma}_n^\dagger\hat{\sigma}_n \otimes \sum_\alpha c_\alpha(\hat{b}_{n,\nu} + \hat{b}_{n,\nu}^\dagger)$, where $c_{n,\nu}$ is the exciton-phonon coupling strength between $n_{\rm th}$ exciton and $\nu_{th}$ phonon mode. The matter dipole operator is expressed as $\hat{\mu} = \sum_n^N \mu_n\left(\hat{\sigma}_n^\dagger + \hat{\sigma}_n\right)$, where $\mu_n$ is the magnitude of the transition dipole of excitation for $n_{\rm th}$ molecule. We use the matter dipole-dipole correlation function to compute the multi-time response functions[26–30] and 2DES spectra.

To interpret the dynamics and spectra, we define the *diabatic* polariton Hamiltonian as $\hat{H}_{\rm pl} \equiv \hat{H} - \hat{H}_{\rm sb} - \hat{H}_b$, with the eigenequation $\hat{H}_{\rm pl}|\alpha\rangle = \epsilon_\alpha|\alpha\rangle$. When only considering the single excitation subspace $|j\rangle = \{|{\rm G}\rangle\otimes|1\rangle \equiv |{\rm G}^1\rangle, |{\rm E}_n\rangle\otimes|0\rangle \equiv |{\rm E}_n^0\rangle\}$(where $|{\rm G}\rangle \equiv \otimes|g_n\rangle$ and $|{\rm E}_n\rangle \equiv |e_n\rangle\otimes|g_m\rangle\ \forall m \neq n$) with degenerate exciton energy $\varepsilon_n = \varepsilon$, and identical light-matter couplings $g_{\rm c}$, $\hat{H}_{\rm pl}$ has well known analytic solution, with two bright polariton states[10,11,31–33]

$$|+\rangle = \cos\Theta_N\Big[\frac{1}{\sqrt{N}}\sum_{n=1}^{N}|{\rm E}_n^0\rangle\Big] + \sin\Theta_N|{\rm G}^1\rangle, \tag{2a}$$

$$|-\rangle = -\sin\Theta_N\Big[\frac{1}{\sqrt{N}}\sum_{n=1}^{N}|{\rm E}_n^0\rangle\Big] + \cos\Theta_N|{\rm G}^1\rangle, \tag{2b}$$

where the mixing angle is $\Theta_N = \frac{1}{2}\tan^{-1}[\frac{2\sqrt{N}\hbar g_{\rm c}}{\hbar\omega_{\rm c}-\varepsilon}]$ and $\Theta_N \in [0, \frac{\pi}{2})$, and $N-1$ dark states with $k \in \{1, \cdots, N-1\}$

$$|{\rm D}_k\rangle = \frac{1}{\sqrt{N}}\sum_{n=0}^{N-1}\exp\left(2\pi i\frac{nk}{N}\right)|{\rm E}_n^0\rangle, \tag{3}$$

The polariton states have the energy of $\varepsilon_\pm = \frac{1}{2}(\varepsilon+\hbar\omega_c) \pm \frac{1}{2}\sqrt{(\varepsilon-\hbar\omega_c)^2+4N\hbar^2 g_c^2}$, whereas the dark states' energy $\varepsilon_{D_k} = \varepsilon$ remains the same as the exciton energy. The eigenenergies of polariton states are split from the original exciton energy. For the zero-detuning case $\varepsilon = \hbar\omega_c$, the Rabi splitting is $\hbar\Omega_R = \varepsilon_+ - \varepsilon_- = 2\sqrt{N}\hbar g_c$, and the strong coupling limit[11,25] is achieved when $\Omega_R \gg \frac{1}{2}(\Gamma+\kappa)$, where $\Gamma$ is the cavity loss rate (linewidth of the cavity transmission spectra, $\tau_c = 1/\Gamma$ is the cavity lifetime) and $\kappa$ is the exciton linewidth. Detailed discussions related to the polariton population relaxation[10? ,11] and decoherence[9] can be found in previous work. The Hamiltonian in Eq. 1 does not include cavity loss, which corresponds to the far field radiation modes coupling to the cavity mode $\{\hat{a}^\dagger, \hat{a}\}$ (see Appendix E in Ref.[20]). Here, we treat the cavity loss through stochastic Lindblad dynamics. For a cavity loss rate $\Gamma$, the quality factor is defined as $Q = \omega_c/\Gamma$.

## III. POLARON DECOUPLING EFFECT

Herrera and Spano[7,8,34] had shown that strong collective resonant coupling of a cavity field with $N$ exciton transitions can effectively decouple exciton-phonon couplings in a disordered molecular ensemble. This is because the coupling strength is re-scaled as $c_\alpha/\sqrt{N}$ for the system bath coupling terms associated with the polariton states $|+\rangle$ and $|-\rangle$, see SI for details. In order to understand the role of vibrational phonons on polariton relaxation process, we express $\hat{H}_{sb}$ in the polaritonic basis $\hat{H}_{sb} = \hat{\mathcal{H}}_\pm + \hat{\mathcal{H}}_{\{\pm,D\}} + \hat{\mathcal{H}}_D$, where $\hat{\mathcal{H}}_\pm$ provides the phonon-mediated transitions between $|+\rangle$ and $|-\rangle$ states, $\hat{\mathcal{H}}_{\{\pm,D\}}$ provides the phonon-mediated transitions between the $|\pm\rangle$ states to the dark state manifolds $\{|D_k\rangle\}$, and $\hat{\mathcal{H}}_D$ provides the phonon-mediated transitions among dark states. Under the resonance condition $\hbar\omega_c = \varepsilon$, $\hat{\mathcal{H}}_\pm$ is expressed as follows[9–11]

$$\hat{\mathcal{H}}_\pm = \frac{1}{2}\Big(|+\rangle\langle+| + |-\rangle\langle-|\Big) \otimes \sum_\alpha \frac{c_\alpha}{\sqrt{N}}(\hat{b}_{0,\nu} + \hat{b}^\dagger_{0,\nu}) \quad (4)$$
$$- \frac{1}{2}\Big(|+\rangle\langle-| + |-\rangle\langle+|\Big) \otimes \sum_\alpha \frac{c_\alpha}{\sqrt{N}}(\hat{b}_{0,\nu} + \hat{b}^\dagger_{0,\nu}),$$

where $\hat{b}_{k,\nu} = \frac{1}{\sqrt{N}}\sum_{n=1}^{N} \exp\big(-2\pi i \frac{nk}{N}\big)\hat{b}_{n,\nu}$ and $\hat{b}^\dagger_{k,\nu} = \frac{1}{\sqrt{N}}\sum_{n=0}^{N-1} \exp\big(-2\pi i \frac{nk}{N}\big)\hat{b}^\dagger_{n,\nu}$ are the creation and annihilation operators of the $\nu_{th}$ bath phonon mode for the $k_{th}$ eigenstates of $\hat{H}_s$. From Eq. 4, one can see that both $|+\rangle$ state and $|-\rangle$ state are *only* coupled to the symmetrical phonon modes (with $k=0$) $\hat{R}_{0,\nu} = (\hat{b}_{\alpha,0} + \hat{b}^\dagger_{\alpha,0})/\sqrt{2\omega_\alpha}$, for both the diagonal term (Holstein coupling) and off-diagonal term (Peierls coupling), with a re-scaled coupling strength $c_\alpha/\sqrt{N}$. Note that the displacement between the $|G^0\rangle$ and the $|\pm\rangle$ states is given by[8] $\mathcal{R}_{\alpha,0} = R_{\alpha,0}/2\sqrt{N}$, where $R_{\alpha,0} = \sqrt{2c_\alpha^2/\omega_\alpha^3}$ is the displacement between the $|E^0_n\rangle$ and $|G^0\rangle$ states. Thus, the effective reorganization energy $\lambda_N = \frac{1}{2}\sum_\alpha \omega_\alpha^2 \mathcal{R}^2_{\alpha,0}$ between the $|G^0\rangle$ state and the $|\pm\rangle$ states is

$$\lambda_N = \frac{\lambda}{4N}. \quad (5)$$

Under the large $N$ limit, the phonon couplings to the $|\pm\rangle$ are effectively decoupled[8] by $\propto 1/N$. For experiments that couple organic molecules with cavity[35,36], $N \sim 10^6 - 10^{12}$. For the recent experiments that couple inorganic nanocrystals inside the cavity (*e.g.*, CdSe Nanoplatelets)[13–16], the typical number of emitters is $N \sim 10^3 - 10^4$. As such, the optical lineshape (such as polariton absorption) that corresponds to $|G,0\rangle \rightarrow |\pm\rangle$ optical transition will become much narrower than systems outside the cavities[8,11], and the same effect will also show up in the diagonal peaks of the 2DES spectra[2]. Due to the computational cost, we only use a small number of molecules ($N \leq 8$) in the simulations. In our previous work[9], we have found that the population decay dynamics and decoherence are largely controlled by the collective quantity $\sqrt{N}g_c$. As long as $N$ is large enough to ensure a density of states for the dark manifold, one can generate nearly identical quantum dynamics by scaling up $g_c$ with a reduced $N$.

The exciton-phonon coupling term also mediates the transitions between $|\pm\rangle$ and the dark state manifold. Under the resonant condition, these coupling terms are expressed as

$$\hat{\mathcal{H}}_{\{\pm,D\}} = \sum_{k=1}^{N-1} |D_k\rangle\langle+| \otimes \sum_\alpha \frac{c_\alpha}{\sqrt{2N}}(\hat{b}_{\alpha,k} + \hat{b}^\dagger_{\alpha,-k}) \quad (6)$$
$$- \sum_{k=1}^{N-1} |D_k\rangle\langle-| \otimes \sum_\alpha \frac{c_\alpha}{\sqrt{2N}}(\hat{b}_{\alpha,-k} + \hat{b}^\dagger_{\alpha,k}) + \text{h.c.},$$

These terms facilitate the transition $|+\rangle \rightarrow \{|D_k\rangle\}$, which is responsible for both population decay and the decoherence of $\rho_{+-}(t)$[9].

## IV. 2DES SPECTRA EXPRESSION

Within the linear response limit, the 2D electronic spectra can be obtained by computing the $3_{rd}$ order response from the four-point correlation function[17,21]

$$R^{(3)}(t_1,t_2,t_3)$$
$$= \text{Tr}\Big[\hat{\mu}(t_3+t_2+t_1)\hat{\mu}^\times(t_2+t_1)\hat{\mu}^\times(t_1)\hat{\mu}^\times(0)\hat{\rho}^{(g)}\Big] \quad (7)$$

where $\hat{\mu}^\times \hat{A} \equiv [\hat{\mu}, \hat{A}]$, and $\hat{\rho}^{(g)}$ is the equilibrium ground state density matrix of the system[18]. Here, the system is perturbed by external laser pulses at times $t_0$, $t_1$, and $t_1+t_2$, and the system response is detected at $t_1+t_2+t_3$. The purely-absorptive 2D spectra is computed by adding the rephasing (denoted as $R^{(3)}_{rep}$) and non-rephasing (denoted

as $R^{(3)}_{\rm nrp}$) contributions expressed as follows

$$R^{(3)}_{\rm rep}(t_1,t_2,t_3) = R^{(3)}_2 + R^{(3)}_3 + R^{(3)*}_1, \tag{8a}$$

$$R^{(3)}_{\rm nrp}(t_1,t_2,t_3) = R^{(3)}_1 + R^{(3)}_4 + R^{(3)*}_2. \tag{8b}$$

In Eq.8a and Eq.8b, the terms on the right-hand side are arranged as individual contributions from (in the order of) Stimulated Emission (SE), Ground State Bleach (GSB), and Excited State Absorption (ESA) signals, respectively. The 2D spectra in the frequency domain are obtained by performing the following Fourier transforms for both rephasing and non-rephasing signals[17,37],

$$R^{(3)}_{\rm rep}(\omega_1,t_2,\omega_3) = \int_0^{T_1} dt_1 \int_0^{T_3} dt_3 R^{(3)}_{\rm rep} e^{i(\omega_3 t_3 - \omega_1 t_1)} S_1 S_3, \tag{9a}$$

$$R^{(3)}_{\rm nrp}(\omega_1,t_2,\omega_3) = \int_0^{T_1} dt_1 \int_0^{T_3} dt_3 R^{(3)}_{\rm nrp} e^{i\omega_3 t_3 + i\omega_1 t_1} S_1 S_3, \tag{9b}$$

where $S_i(t_i) = \cos(\pi t_i/2T_i)$ is a smoothing function for time $t_i$. The frequency domain pure absorptive 2D spectra are the imaginary part of the total contribution from rephasing (Eq. 9a) and non-rephasing (Eq. 9b) signals, expressed as follows

$$R^{(3)}(\omega_1,t_2,\omega_3) = -\Im\mathfrak{m}\left[R^{(3)}_{\rm rep}(\omega_1,t_2,\omega_3) + R^{(3)}_{\rm nrp}(\omega_1,t_2,\omega_3)\right]. \tag{10}$$

We use our previously developed $\mathcal{L}$-PLDM[17–19,21] approach to simulate polariton 2DES spectra. For efficient simulation of 2DES of polaritonic systems with $N$ molecules, we use the recently developed computational algorithms[18,19] that significantly reduce the numerical cost by taking advantage of the sparsity and the symmetry of the HTC Hamiltonian.

## V. RESULTS AND DISCUSSION

We present numerical simulations of the polariton 2DES spectra for $N$-molecules collectively coupled to a single cavity mode. We investigate how collective light–matter interactions influence these nonlinear optical signals, including spectral features that reveal linewidth narrowing, enhanced coherence lifetimes, and signatures of polaron decoupling.

## VI. 2DES SPECTRA

Fig. 2 shows the simulated pure-absorptive 2DES for $N = 4$ molecules coupled to a single cavity mode, at various population times $t_2$. The light–matter coupling strength for each molecule is fixed at $\hbar g_{\rm c} = 200$ cm$^{-1}$ ($\approx$ 24.8 meV), and the collective coupling produces the lower (LP) and upper polaritons (UP) peaks at $\hbar\omega_- \approx -50$ meV and $\hbar\omega_+ \approx 50$ meV, respectively, with respect to the molecular excitation energy $\varepsilon$. This results in a Rabi-Splitting, $\hbar\Omega_{\rm R} = \hbar\omega_+ - \hbar\omega_- \approx 100$ meV. The cavity loss rate is set to $\Gamma_{\rm c} = 10$ meV. Each molecule is coupled to a harmonic bath, characterized by a reorganization energy $\hbar\lambda_{\rm b} = 50$ cm$^{-1}$ ($\approx$ 6.2 meV) and a characteristic frequency, $\hbar\omega_{\rm b} = 18$ cm$^{-1}$ ($\approx$ 2.2 meV). These parameters are consistent with the experimental values for CdSe Nanoplatelets[15] and have been used in previous theoretical polariton spectra simulations[17–19].

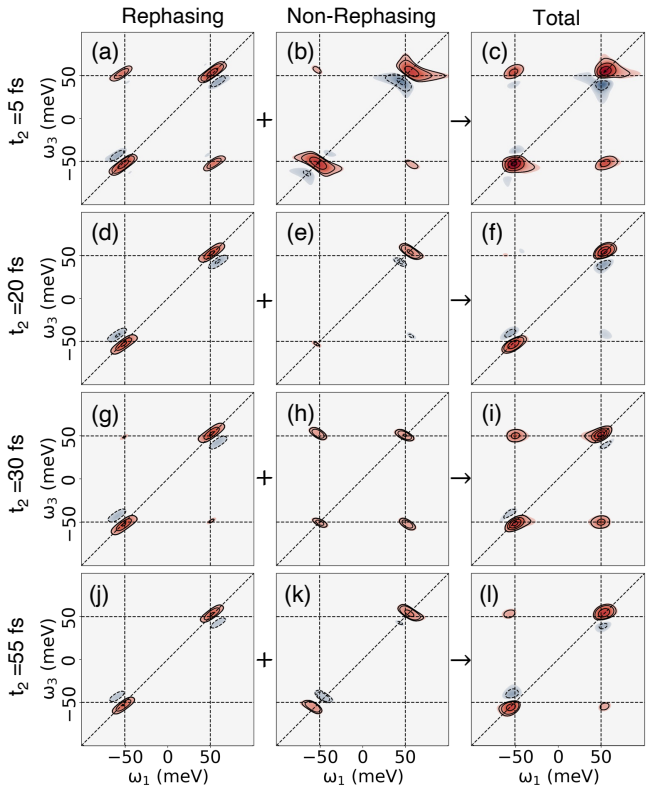


FIG. 2. 2DES signal breakdown for $N = 4$ molecules coupled to cavity. The left column presents the rephasing contribution, the middle column presents the non-rephasing signals, and the third column represents the total pure-absorptive 2DES. The rows indicate the population times at $t_2 = 5$ fs, 20 fs, 30 fs, and 55 fs, respectively.

The first column of Fig. 2 shows the rephasing contribution to the pure-absorptive 2DES as a function of the population time $t_2$. In Fig. 2(a), two prominent diagonal peaks are observed at $(\omega_-, \omega_-)$ and $(\omega_+, \omega_+)$, corresponding to the lower and upper polariton states, respectively. Both peaks exhibit elongations along the diagonal, a hallmark of inhomogeneous broadening due to slow environmental fluctuations caused by low-frequency bath modes. Additionally, negative features appear along the diagonal peaks, due to excited-state absorption (ESA) transitions originating from the polariton states to the doubly excited manifold during the third laser inter-

action[19]. Cross peaks appear at ($\omega_+$, $\omega_-$) and ($\omega_-$, $\omega_+$), which oscillate over $t_2$, indicating a coherent energy transfer between the upper and lower polariton states (due to the light-matter coupling between $|G^1\rangle$ and $|E_n^0\rangle$) via the $|+\rangle\langle-|$ and $|-\rangle\langle+|$ pathways, respectively.

Fig. 2(b) shows the non-rephasing contribution of polariton 2DES spectra at $t_2 = 5$ fs. Similar to the rephasing case (in Fig. 2(a)), two diagonal peaks are visible, corresponding to the upper ($|+\rangle\langle+|$) and lower ($|-\rangle\langle-|$) polariton population states. Unlike the rephasing contributions, these diagonal peaks in the non-rephasing signals are elongated along the anti-diagonal direction, reflecting homogeneous broadening from fast environmental fluctuations. In this case, the broadening is dominated by contributions from high-frequency intramolecular vibrations and cavity photon loss. Cross-peaks appear at ($\omega_-$, $\omega_+$) and ($\omega_+$, $\omega_-$) are associated with coherence pathways which involve the $|-\rangle\langle+|$ and $|+\rangle\langle-|$ states respectively. These cross-peaks are noticeably weaker in intensity than those in the rephasing signal, primarily due to the absence of stimulated emission pathways in the non-rephasing process and partial cancellation from overlapping ESA contributions [19].

Fig. 2(c) shows the pure-absorptive 2DES signal, obtained by summing the rephasing (panel a) and non-rephasing (panel b) contributions (see Eq. 10). The diagonal peaks at ($\omega_-$, $\omega_-$) and ($\omega_+$, $\omega_+$) corresponding to the lower $|-\rangle\langle-|$ and upper $|+\rangle\langle+|$ polariton population states, respectively, appear relatively flattened along the excitation axis, $\omega_1$, indicating a partial cancellation of the inhomogeneous broadening exhibited in the rephasing signal by the anti-diagonally elongated diagonal signal from the non-rephasing contribution. The cross-peaks, by contrast, remain diagonally elongated, suggesting that coherence-mediated energy transfer between the polariton states is predominantly governed by the rephasing pathways.

Figs. 2(a), (d), (g), and (j) show the evolution of the rephasing signal at increasing population times $t_2$. As $t_2$ progresses, the diagonal peak intensities gradually diminish, reflecting population decay from the polariton states due to cavity loss at a rate of $\Gamma_c$. The overall shape remains diagonally elongated due to a persistent inhomogeneous broadening. More notably, the cross-peak intensities exhibit oscillations with a frequency corresponding to the Rabi splitting ($\Omega_R = \omega_+ - \omega_-$), signaling coherent energy exchange between upper and lower polariton states. These oscillations decay over time due to dephasing from both molecular vibrations and cavity loss. The decay of the polariton coherence $|+\rangle\langle-|$ (and $|-\rangle\langle+|$) will be further quantified in Fig. 3.

Figs. 2(b), (e), (h), and (k) show the non-rephasing contributions at different $t_2$ delays. Based on the analysis from the Feynman diagrams/Liouville pathways (see Fig. S3 in SI), stimulated emission (SE) signals do not give rise to any cross-peaks. Further, the ground-state bleach (GSB) and excited-state absorption (ESA) contributions are expected to completely cancel each other when transition frequencies between the different manifolds are the same. Here, however, we still observe oscillatory cross-peaks that do not fully vanish in the non-rephasing signals. This surviving off-diagonal signal arises from a partial cancellation between ESA and GSB due to a mismatch in transition frequencies between the ground-to-first-excited manifold and the first-to-second-excited manifold (see Fig. S2 in *SI*). In contrast to the cross peaks, the diagonal peaks exhibit pronounced oscillations, caused by the presence of $|+\rangle\langle-|$ (and $|-\rangle\langle+|$) coherences during $t_2$ in the non-rephasing signal. For the diagonal peaks, these coherence pathways are not present in the rephasing pulse sequence[38–41] and only show up in the non-rephasing pulse sequence. This can be directly verified by inspecting the corresponding Feynman diagrams, where detailed analysis of different peaks and oscillations is provided in the Supporting Information (SI).

Figs. 2(c), (f), (i), and (l) present the total pure-absorptive 2DES at various $t_2$. The cross-peaks exhibit pronounced beating patterns accompanied by evolving lineshapes. Notably, the diagonal peaks, which are initially flattened at $t_2 = 5$ fs [see panel 2(c)], become diagonally elongated by $t_2 = 20$ fs [panel (f)]. This transient feature arises because the system starts in an uncorrelated tensor product state of the polaritonic ground state and a thermal distribution of vibrational modes (due to the Franck-Condon excitation), and requires a finite time to build up system–bath correlations[29]. Following this initial rise, the system undergoes spectral diffusion[26,29], causing the diagonal peaks to gradually flatten as seen at $t_2 = 55$ fs. Also, unlike the non-rephasing spectra, we observe that the diagonal peaks do not fluctuate much, indicating that the signal is dominated by rephasing processes.

## VII. COHERENCE ENHANCEMENT

The cross-peaks in the pure-absorptive 2DES provide a direct measure of coherent oscillations between upper and lower polariton states. In Fig. 3, we track the time-dependent oscillations of the lower cross-peak from the 2DES for systems where $\Omega_R$ increases by raising $N$ while keeping $g_c$ constant. The cyan, orange, and red curves in panels (a)-(c) correspond to the $t_2$-dependent oscillations of the lower cross-peak intensity for $\hbar\sqrt{N}g_c = 35$ meV, 50 meV, and 70 meV, respectively. As $\Omega_R = 2\sqrt{N}g_c$ increases, the coherence oscillations become faster and persist longer in time, as observed in our previous theoretical studies[9]. To extract the coherence lifetime, follow the previous theoretical investigation on polariton coherence[9]

$$R^{(3)}(\omega_1, t_2, \omega_3) \propto \mathrm{Re}[\rho_{+-}(t_2)] \sim \frac{1}{2}\cos(\Omega_R \cdot t_2) \cdot e^{-t_2/\tau}, \tag{11}$$

where the $\rho_{+-}(t_2)$ coherence oscillates with the Rabi frequency $\Omega_R \cdot t_2$ and decay exponentially as $e^{-t_2/\tau}$, with

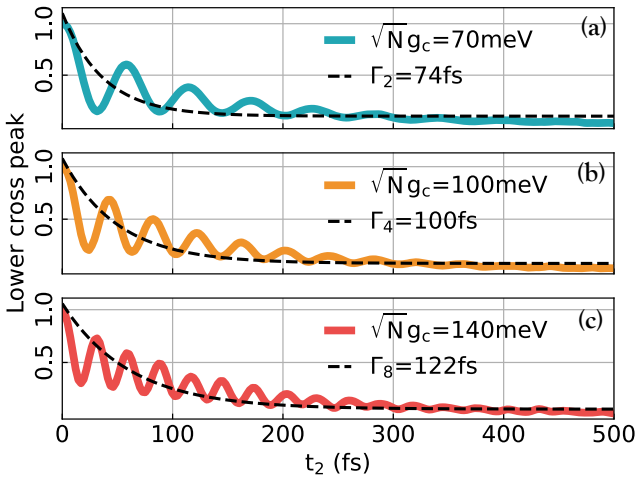


FIG. 3. Lower Cross peak oscillations in 2DES of N-molecules coupled to the cavity. In Panels (a), (b), and (c), the cyan, orange, and red curves represent the cross-peak oscillation for $N = 2$, 4, and 8 molecules coupled to a cavity mode, respectively. The black dotted lines in all the panels represent the lifetime curve fit (with Eq. 11) for the respective curves.

$\tau$ as the coherence lifetime. This expression was shown to provide an excellent fit to the numerically exact coherence obtained from the quantum dynamics simulations[9]. Here, we focus on the $R^{(3)}(\omega_1, t_2, \omega_3)$ signal, with $\omega_1 = 50$ meV and $\omega_3 = -50$ meV, and with the black dashed lines in Fig. 3 showing the exponential decay envelope. We observe that the coherence time $\tau$ increases with $\Omega_{\rm R}$, consistent with prior theoretical results[9]. The rising oscillation frequency across panels (a)–(c) reflects the increased Rabi splitting $\Omega_{\rm R}$ with larger $N$, under a fixed single-molecule coupling strength $g_{\rm c}$.

As shown in our previous work[9], the main mechanism of $\rho_{+-}(t) = c_+^*(t)\cdot c_-(t)$ decay in HTC type Hamiltonian is due to the decrease of $c_+^*(t)$ (because of the UP population $\rho_{++}(t) = c_+^*(t)\cdot c_+(t)$ decay to the dark states), while $c_-(t)$ does not have a significant change. The main contribution of the decoherence of $\rho_{+-}(t)$ originates from the population decay from the $|+\rangle$ state to the dark states manifold $\{|{\rm D}_k\rangle\}$. This population decay is caused by the phonon coupling term $\hat{\mathcal{H}}_{\{\pm,{\rm D}\}}$ in Eq. 6. One can thus estimate the coherence time $T_2$ as follows

$$\frac{1}{\tau} \approx \frac{1}{2}k_{+\to{\rm D}} + \frac{1}{2}\tau_{\rm c}^{-1} \tag{12}$$

where $k_{+\to{\rm D}}$ is the population decay for the process $|+\rangle \to \{|{\rm D}_k\rangle\}$, The rate $k_{+\to{\rm D}}$ can be estimated using Fermi's Golden Rule (FGR) as follows

$$k_{+\to{\rm D}} = \frac{N-1}{N}\cdot J(\sqrt{N}g_{\rm c})\cdot\left[\bar{n}(\sqrt{N}g_{\rm c})+1\right], \tag{13}$$

where $J(\omega)$ is the phonon spectral density expressed in Eq. 19, and $\bar{n}(\omega) = 1/(e^{\beta\hbar\omega}-1)$ is the Bose-Einstein distribution function of the phonon. Note that the energy gap between $|+\rangle$ and $|{\rm D}_k\rangle$ is $\omega_+ - \omega_{\rm D} = \Omega_{\rm R}/2 = \sqrt{N}g_{\rm c}$, which appears in $J(\omega)$ and $\bar{n}(\omega)$ of the FGR expression. For an arbitrary detuning case, there will be an additional factor $[1+\cos(2\Theta_N)]$ in the FGR expression, see Eq. S21c in Ref. 9. Eq. 12-13 successfully explained the scaling of $\tau$ with respect to $N$ and $g_{\rm c}$ for $\rho_{+-}(t)$. In particular, as increasing the $\Omega_{\rm R} = 2\sqrt{N}g_{\rm c}$, the decay rate $k_{+\to{\rm D}}$ slows down, leading to a longer coherence time for $\rho_{+-}(t)$. Fig. 3 confirm this prediction and indeed suggests a longer coherence time can be achieved by increasing $\Omega_{\rm R}$.

For the early time of the coherence cross peak shown in Fig. 3, as we increase $N$ thus increasing $\sqrt{N}g_{\rm c}$, the behavior of decoherence changes from a Gaussian-type (see Fig. 3a for $t_2 < 20$ fs) to a more Lorentzian-type (see Fig. 3c) behaviour[9,11]. This type of transition was theoretically explained in Ref. 9, due to the transition from the phonon bath dominating regime (which is inhomogeneous) to a cavity loss dominating case (homogeneous). This can also be observed from the 2DES linshapes for these cases, with details in SI.

## VIII. POLARON DECOUPLING EFFECT FROM 2DES

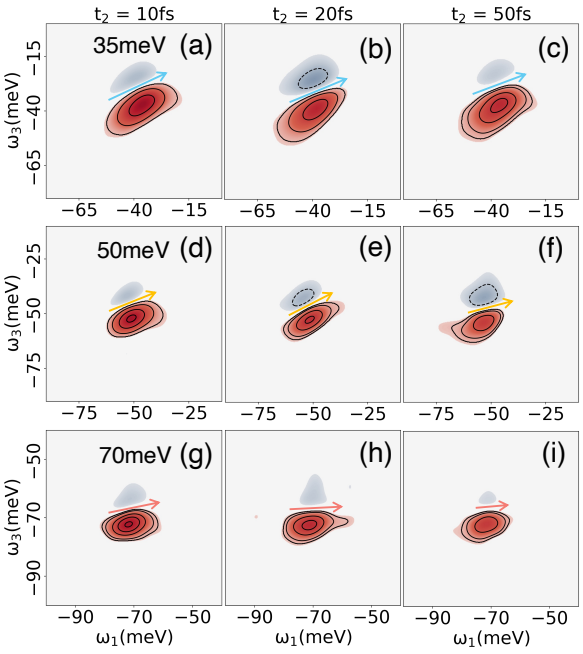


FIG. 4. Lower polariton pure-absorptive 2D spectra peak for various collective coupling stregnths. Panels (a)-(c) represent the LP diagonal peak for $t_2$= 10fs, 20fs and 50fs respectively for $\sqrt{N}g_{\rm c} = 35$ meV. The blue arrow shows the nodal line at each $t_2$. Panels (d)-(f) represent the LP lineshape for $t_2$= 10fs, 20fs, and 50fs, respectively, for $\sqrt{N}g_{\rm c} = 50$ meV with the yellow line indicating the nodal line at each $t_2$. Panels (g)-(i) represent the LP peak at different population times, with the red line representing the nodal line for $\sqrt{N}g_{\rm c} = 70$ meV.

While the relative widths of diagonal and anti-diagonal features in a 2DES provide insight into spectral inhomogeneity, a more direct probe of exciton–phonon coupling strength is given by the nodal line slope (NLS) of the diagonal peaks[2,26,29,42]. In particular, an NLS that tilts toward the excitation axis indicates weaker coupling and reduced system-bath interaction. Recent experiments by Watanabe *et al.*[2] demonstrated that, in the strong coupling regime, increasing the number of molecules per cavity mode volume leads to a flattening of the lower polariton (LP) diagonal peak.

Figure 4 shows the time evolution of the LP 2D lineshapes and their corresponding nodal line slopes (NLS) for systems with $\sqrt{N}g_c = 35$ meV, 50 meV, and 70 meV (with $N = 2, 4, 8$ accordingly). Panels (a)-(c) display the diagonal LP peak for $\sqrt{N}g_c = 35$ meV, with the blue arrow indicating the nodal line between the ESA and GSB+SE features. The LP 2DES lineshape maintains a visibly slanted NLS, reaching a peak value of 20° at around $t_2$=50 fs. Panels (d)-(f) are the LP peaks for $\sqrt{N}g_c = 50$ meV, and the yellow arrow is the nodal line. In this case, the NLS changes from 15° at $t_2 = 10$ fs to around 10° at $t_2 = 50$ fs, indicating a faster spectral diffusion and an increased polaron decoupling effect compared to the $\sqrt{N}g_c = 35$ meV case. For the case of$\sqrt{N}g_c = 70$ meV, shown in panels (g)-(i), the red NLS line starts nearly flat at 6°, and further reduces to 4°, consistent with strong suppression of system–bath interactions via the polaron decoupling mechanism[2,8,11] in the collective regime.

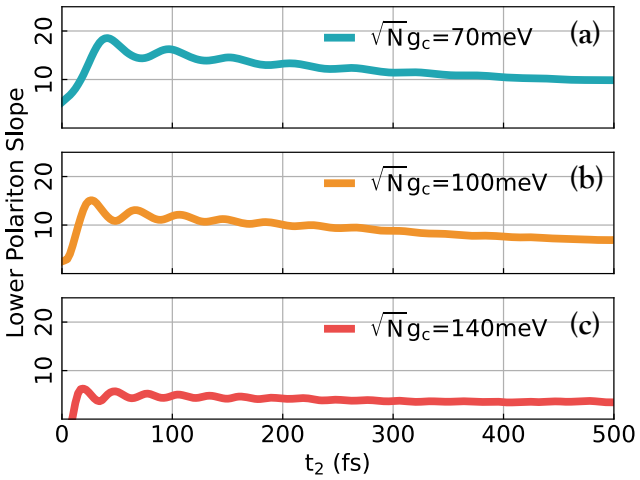


FIG. 5. Slope between ESA and GSB+SE signals in the LP diagonal peak of pure-absorptive 2D spectra for different $N$-molecule polariton system, as a function of population time $t_2$.

Figure 5 presents the NLS between ESA and GSB+SE signals as $t_2$ varies for different $\sqrt{N}g_c$ values. In panel (a), for $\sqrt{N}g_c$=35 meV, the cyan curve peaks at ≈ 19° around $t_2$=40 fs, staying above 10° even at 500 fs, indicating strong exciton–phonon coupling and slow spectral diffusion. In panel (b), for $\sqrt{N}g_c$=50 meV, the orange curve peaks at 16° at $t_2 = 20$ fs but drops to ≈ 7° by 500 fs, suggesting faster spectral diffusion and reduced system–bath interaction. In panel (c), for $\sqrt{N}g_c$=70 meV, the red curve starts at ≈ 6° at $t_2$=10 fs and decreases to 4° at 500 fs. Although the rate of spectral diffusion is slower than in the $\sqrt{N}g_c$=50 meV case, the overall polariton–phonon coupling is significantly reduced. For $\sqrt{N}g_c$=70 meV , the initial slope is about one-fourth of that for $\sqrt{N}g_c$=35 meV and one-third of $\sqrt{N}g_c$=50 meV, nearing 0°, indicating near-complete polaron decoupling in the collective limit.

## IX. CONCLUSION

We use state-of-the-art quantum dynamics simulations to investigate polaritonic nonlinear spectroscopy under the collective coupling regime. Our approach is able to capture both non-Markovian bath effects from the molecular environment and the Markovian type of cavity loss[17–19,21]. For the first time, we are able to simulate the $N$-dependent non-perturbative (in system-bath interaction) non-Markovian non-linear spectra, which are very difficult for other widely used Markovian and perturbative approaches due to the exponential increase of computational cost of the increasing Hilbert space (and consecutively the Liouville space) in the second excitation manifold with increasing $N$.

Our theoretical results reveal that as the number of molecules $N$ that collectively couple to the cavity increases, the Rabi splitting scales as $2\sqrt{N}g_c$ and the polariton linewidths narrow, eventually saturating at the cavity's homogeneous half-linewidth. Additionally, we observed that as $N$ increases, both the diagonal peaks and cross-peaks tend to flatten progressively. Time-resolved analysis of cross-peak oscillations in the pure-absorptive 2DES reveals enhanced coherence lifetimes as $N$ increases. This trend reflects the suppression of decoherence pathways via collective coupling[9]. Moreover, the nature of dephasing shifts from inhomogeneous (Gaussian-like) at small $N$, dominated by exciton–phonon interactions, to homogeneous (Lorentzian-like) at large $N$, where photonic loss becomes the dominant decay mechanism.

The enhancement of coherence is directly correlated with the reduction of the effective reorganization energy of the polariton states. We directly characterize this polaron decoupling effect by calculating the nodal line slope (NLS) between the negative ESA and positive GSB+SE signals in the lower polariton peak of the 2D spectra. The increase in $N$ (number of molecules collectively coupled to the cavity, thus the collective light-matter coupling magnitude and Rabi Splitting) flattens the NLS with respect to the excitation axis, and the slope becomes closer to the full spectral diffusion limit, as previously experimentally observed by Takahashi *et al.*[2]. This work demonstrates that with a realistic range of re-

organization energy for the CdSe Nanoplatelets coupled to the optical cavity, one could generate unprecedented long-lived coherence at room temperature, up to 300-500 fs between UP and LP states, when the hybrid system is reaching a collective coupling strength of $\sqrt{N}g_c = 70$ meV. This collective light-matter coupling strength has been realized in our recent experimental setup[13–16]. Our work provides fundamental insights into the polariton photodynamics in the context of non-linear spectra, spectra diffusion, coherence, and decoupling from vibrational environment, and paves the way for future applications of polaritons in Quantum Information Science.

## X. APPENDIX

### A. Theory for 2DES Signals

The nonlinear responses in Eq. 7 can be equivalently expressed as[21]

$$R^{(3)}(t_1,t_2,t_3) = -i\mathrm{Tr}\left[\hat{\mu}\mathcal{G}_3\left(\hat{\mu}^{\times}\mathcal{G}_2\left(\hat{\mu}^{\times}\mathcal{G}_1\left(\hat{\mu}_0^{\times}\hat{\rho}^{(g)}\right)\right)\right)\right], \tag{14}$$

where $\mathcal{G}_j\hat{A} = e^{\frac{i}{\hbar}\hat{H}t_j}\hat{A}e^{-\frac{i}{\hbar}\hat{H}t_j}$. These expressions in Eq. 14 can be easily evaluated by using the PLDM approximation[21], where the path-integral expression for the forward and backward propagators are used and the partial linearization approximation on the nuclear DOF is applied[22,23]. For $R^{(3)}$, the PLDM approximation is expressed as[21]

$$\begin{aligned} &R^{(3)}(t_1,t_2,t_3) \qquad (15)\\ &\approx -i\sum_{n_3}\sum_{n_2,\tilde{n}_2}\int d\tau_2[\hat{\mu}\tilde{\rho}^{(3)}]_{n_3,n_3}\sum_{n_1,\tilde{n}_1}\int d\tau_1[\hat{\mu}^{\times}\tilde{\rho}^{(2)}]_{n_2,\tilde{n}_2}\\ &\quad\times\sum_{n_0,\tilde{n}_0}\int d\tau_0[\hat{\mu}^{\times}\tilde{\rho}^{(1)}]_{n_1,\tilde{n}_1}[\hat{\mu}\hat{\rho}_g]_{n_0,\tilde{n}_0}\cdot[\hat{\rho}_{\mathrm{b}}]_{\mathrm{w}}. \end{aligned}$$

In Eq.7, $R^{(3)}$ can be separated into 8 different Liouville pathways, each can be categorized as either rephasing or non-rephasing signals. Four of these Liouville pathways correspond to

$$R_1^{(3)} = -i\mathrm{Tr}[\hat{\mu}(t_3+t_2+t_1)\hat{\mu}(0)\hat{\rho}_g\hat{\mu}(t_1)\hat{\mu}(t_1+t_2)], \tag{16a}$$

$$R_2^{(3)} = -i\mathrm{Tr}[\hat{\mu}(t_3+t_2+t_1)\hat{\mu}(t_1)\hat{\rho}_g\hat{\mu}(0)\hat{\mu}(t_2+t_1)], \tag{16b}$$

$$R_3^{(3)} = -i\mathrm{Tr}[\hat{\mu}(t_3+t_2+t_1)\hat{\mu}(t_2+t_1)\hat{\rho}_g\hat{\mu}(0)\hat{\mu}(t_1)], \tag{16c}$$

$$R_4^{(3)} = -i\mathrm{Tr}[\hat{\mu}(t_3+t_2+t_1)\hat{\mu}(t_2+t_1)\hat{\mu}(t_1)\hat{\mu}(0)\hat{\rho}_g], \tag{16d}$$

while the other four pathways can be constructed from the complex conjugate of Eq.16a to Eq.16d. Similar to Eq. 15, the individual Liouville pathways in Eq. 16 can also be expressed in the PLDM response function formalism,

### B. Details of Cavity Loss Dynamics

The cavity loss channel from state $|\mathrm{G}^1\rangle$ to state $|\mathrm{G}^0\rangle$ can be described by the loss operator

$$\hat{L} = |\mathrm{G}^0\rangle\langle\mathrm{G}^1|. \tag{17}$$

The dissipator $\mathcal{L}_{\hat{L}}$ accounts for the cavity loss channel, causing the system to relax

$$\mathcal{L}_{\hat{L}}[\hat{\rho}_{\mathrm{Q}}] = \Gamma\Big(\hat{L}\hat{\rho}_{\mathrm{Q}}\hat{L}^{\dagger} - \frac{1}{2}\{\hat{L}^{\dagger}\hat{L},\hat{\rho}_{\mathrm{Q}}\}\Big), \tag{18}$$

where $\Gamma$ is the rate of relaxation of the jump operator which quantifies the coupling strength of the system to the environment, and $\{\hat{A},\hat{B}\} = \hat{A}\hat{B}+\hat{B}\hat{A}$ is the anti-commutator, and $\hat{\rho}_{\mathrm{Q}} = \mathrm{Tr}_{\mathrm{b}}[\hat{\rho}]$ is the reduced density matrix operator for the quantum subsystem by tracing out all bath DOF. Eq/ 18 was simulated using the stochastic Lindblad approach when combining with the path-integral quantum dynamics approaches, detailed in Ref.[17]. In this study, $\Gamma$ is the cavity loss rate, and the cavity quality factor is defined as $\mathcal{Q} = \hbar\omega_c/\Gamma$

### C. Details of Model Systems

The system-bath interactions are determined by the spectral density[43,44]

$$J(\omega) = \pi\sum_{\alpha}\frac{c_\alpha^2}{2\omega_\alpha}\delta(\omega-\omega_\alpha) = \frac{2\lambda\gamma\omega}{\gamma^2+\omega^2} \tag{19}$$

where we use the Drude-Lorentz model, $\gamma$ is the bath characteristic frequency, and the reorganization energy (inside $\hat{H}_{\mathrm{M}}$) is $\lambda = \sum_\alpha c_\alpha^2/2\omega_\alpha^2 = (1/\pi)\int_0^\infty d\omega\ J(\omega)/\omega$ for all molecules. Here, we use the following parameters: excitation energy $\varepsilon = 2.0$ eV, the bath reorganization energy $\lambda = 50$ cm$^{-1}$, and the bath characteristic frequency $\gamma = 18$ cm$^{-1}$, which are the typical parameters for CdSe Nanoplatelets (see schematic illustration in Fig. 1a) which has been shown to couple strongly to a dielectric optical cavity.[13,14]

### D. Computational Approaches

We applied recently developed theoretical approaches which the efficient calculations of the polariton 2DES spectra using the $\mathcal{L}$-PLDM approach[17–19]. First, we take advantage of sparsity and the symmetry of the HTC Hamiltonian[18], which allows one to reduce the cost of acting the polariton Hamiltonian onto a state vector to the linear order of the number of states, instead of the quadratic order. Second, we apply the Chebyshev series expansion approach for quantum dynamics propagation[18] and simulate the polariton dynamics in the HTC system, allowing one to use a much larger time step for

propagation and only requiring a few recursive operations of the Polariton Hamiltonian acting on state vectors[18]. Third, we apply an efficient importance sampling scheme[19] to compute the sums in Eq. 15 in the PLDM-2DES response function, which allows us to significantly reduce the computational costs[17,19].

## XI. ACKNOWLEDGMENTS

This work was supported by the Department of Energy under Grant No. DE-SC0022171, the National Science Foundation Award under Grant No. CHE-2244683, the University Research Award from the University of Rochester, as well as the University of Rochester Office of the Vice President for Research, the School of Medicine and Dentistry and Arts, Sciences & Engineering via the Center for Integrated Research Computing (CIRC). The work at Boston University was supported by the U.S. Department of Energy, Office of Science, Office of Basic Energy Sciences under Award Number DE-SC0026384 awarded to M.S. M.E.M. appreciates the support from the Messersmith Fellowship by the Department of Chemistry at the University of Rochester. Computing resources were provided by the Center for Integrated Research Computing (CIRC) at the University of Rochester. M.E.M. appreciates valuable discussions and comments from Ben Chng.

## CONFLICT OF INTEREST

The authors have no conflicts of interest to disclose.

## AVAILABILITY OF DATA

The data that support the findings of this study are available from the corresponding author upon a reasonable request.

[1]T. W. Ebbesen, "Hybrid light-matter states in a molecular and material science perspective," Acc. Chem. Res. **49**, 2403–2412 (2016).
[2]S. Takahashi and K. Watanabe, "Decoupling from a thermal bath via molecular polariton formation," J. Phys. Chem. Lett. **11**, 1349–1356 (2020).
[3]S. T. Wanasinghe, A. Gjoni, W. Burson, C. Majeski, B. Zaslona, and A. S. Rury, "Motional narrowing through photonic exchange: Rational suppression of excitonic disorder from molecular cavity polariton formation," J. Phys. Chem. Lett. **15**, 2405–2418 (2024).
[4]E. O. Odewale, S. T. Wanasinghe, and A. S. Rury, "Assessing the determinants of cavity polariton relaxation using angle-resolved photoluminescence excitation spectroscopy," J. Phys. Chem. Lett. **15**, 5705–5713 (2024).
[5]M. Son, Z. T. Armstrong, R. T. Allen, A. Dhavamani, M. S. Arnold, and M. T. Zanni, "Energy cascades in donor-acceptor exciton-polaritons observed by ultrafast two-dimensional white-light spectroscopy," Nature Communications **13**, 7305 (2022).
[6]S. Dhamija and M. Son, "Mapping the dynamics of energy relaxation in exciton–polaritons using ultrafast two-dimensional electronic spectroscopy," Chemical Physics Reviews **5**, 041309 (2024).
[7]F. Herrera and F. C. Spano, "Cavity-controlled chemistry in molecular ensembles," Phys. Rev. Lett. **116**, 238301 (2016).
[8]F. Herrera and F. C. Spano, "Theory of nanoscale organic cavities: The essential role of vibration-photon dressed states," ACS photonics **5**, 65–79 (2018).
[9]B. X. Chng, W. Ying, Y. Lai, A. N. Vamivakas, S. T. Cundiff, T. D. Krauss, and P. Huo, "Mechanism of molecular polariton decoherence in the collective light–matter couplings regime," The Journal of Physical Chemistry Letters **15**, 11773–11783 (2024).
[10]Y. Lai, W. Ying, and P. Huo, "Non-equilibrium rate theory for polariton relaxation dynamics," The Journal of Chemical Physics **161**, 104109 (2024).
[11]W. Ying, M. E. Mondal, and P. Huo, "Theory and quantum dynamics simulations of exciton-polariton motional narrowing," The Journal of Chemical Physics **161** (2024).
[12]R. M. Gracia, G. J. Russo, S. Park, L. Kinziabulatova, and M. Son, "Modulation of vibronic transitions in chlorophyll a through strong light-matter coupling," J. Mater. Chem. C , DOI: 10.1039/D5TC03240G (2025).
[13]L. Qiu, A. Mandal, O. Morshed, M. T. Meidenbauer, W. Girten, P. Huo, A. N. Vamivakas, and T. D. Krauss, "Molecular polaritons generated from strong coupling between cdse nanoplatelets and a dielectric optical cavity," The Journal of Physical Chemistry Letters **12**, 5030–5038 (2021).
[14]O. Morshed, M. Amin, N. M. B. Cogan, E. R. Koessler, R. Collison, T. M. Tumiel, W. Girten, F. Awan, L. Mathis, P. Huo, A. N. Vamivakas, T. W. Odom, and T. D. Krauss, "Room-temperature strong coupling between cdse nanoplatelets and a metal–dbr fabry–pérot cavity," The Journal of Chemical Physics **161**, 014710 (2024).
[15]M. Amin, E. R. Koessler, O. Morshed, F. Awan, N. M. B. Cogan, R. Collison, T. M. Tumiel, W. Girten, C. Leiter, A. N. Vamivakas, P. Huo, and T. D. Krauss, "Cavity controlled upconversion in cdse nanoplatelet polaritons," ACS Nano **18**, 21388–21398 (2024).
[16]F. Freire-Fernández, N. G. Sinai, M. J. Hui Tan, S.-M. Park, E. R. Koessler, T. Krauss, P. Huo, and T. W. Odom, "Room-temperature polariton lasing from cdse core-only nanoplatelets," ACS Nano **18**, 15177–15184 (2024).
[17]M. E. Mondal, E. R. Koessler, J. Provazza, A. N. Vamivakas, S. T. Cundiff, T. D. Krauss, and P. Huo, "Quantum dynamics simulations of the 2d spectroscopy for exciton polaritons," The Journal of Chemical Physics **159** (2023).
[18]M. E. Mondal, A. N. Vamivakas, S. T. Cundiff, T. D. Krauss, and P. Huo, "Polariton spectra under the collective coupling regime. i. efficient simulation of linear spectra and quantum dynamics," The Journal of chemical physics **162** (2025).
[19]M. E. Mondal, A. N. Vamivakas, S. T. Cundiff, T. D. Krauss, and P. Huo, "Polariton spectra under the collective coupling regime. ii. 2d non-linear spectra," The Journal of Chemical Physics **162** (2025).
[20]E. R. Koessler, A. Mandal, and P. Huo, "Incorporating lindblad decay dynamics into mixed quantum-classical simulations," J. Chem. Phys. **157**, 064101 (2022).
[21]J. Provazza, F. Segatta, M. Garavelli, and D. F. Coker, "Semiclassical path integral calculation of nonlinear optical spectroscopy," J. Chem. Theory Comput. **14**, 856–866 (2018).
[22]P. Huo, I. Miller, Thomas F., and D. F. Coker, "Communication: Predictive partial linearized path integral simulation of condensed phase electron transfer dynamics," J. Chem. Phys. **139**, 151103 (2013).
[23]M. Lee, P. Huo, and D. Coker, "Semi-classical path integral dynamics: Photosynthetic energy transfer with realistic environment interactions," Ann. Rev. Phys. Chem. **67**, 639 (2016).
[24]P. Huo and D. F. Coker, "Communication: Partial linearized density matrix dynamics for dissipative, non-adiabatic quantum evolution," The Journal of Chemical Physics **135**, 201101 (2011).

[25]A. Mandal, M. A. Taylor, B. M. Weight, E. R. Koessler, X. Li, and P. Huo, "Theoretical advances in polariton chemistry and molecular cavity quantum electrodynamics," Chemical Reviews **123**, 9786–9879 (2023).
[26]L. Valkunas, D. Abramavicius, and T. Mancal, *Molecular excitation dynamics and relaxation: quantum theory and spectroscopy* (John Wiley & Sons, 2013).
[27]E. Collini, "2d electronic spectroscopic techniques for quantum technology applications," J. Phys. Chem. C **125**, 13096–13108 (2021).
[28]A. M. Brańczyk, D. B. Turner, and G. D. Scholes, "Crossing disciplines-a view on two-dimensional optical spectroscopy," Ann. Phys. **526**, 31–49 (2014).
[29]P. Hamm and M. Zanni, *Concepts and Methods of 2D Infrared Spectroscopy* (Cambridge University Press, 2011).
[30]A. Gelzinis, R. Augulis, V. Butkus, B. Robert, and L. Valkunas, "Two-dimensional spectroscopy for non-specialists," Biochim. Biophys. Acta, Bioenerg. **1860**, 271–285 (2019).
[31]J. A. Campos-Gonzalez-Angulo, R. F. Ribeiro, and J. Yuen-Zhou, "Generalization of the tavis–cummings model for multilevel anharmonic systems," New Journal of Physics **23**, 063081 (2021).
[32]C. A. DelPo, B. Kudisch, K. H. Park, S.-U.-Z. Khan, F. Fassioli, D. Fausti, B. P. Rand, and G. D. Scholes, "Polariton transitions in femtosecond transient absorption studies of ultrastrong light–molecule coupling," The journal of physical chemistry letters **11**, 2667–2674 (2020).
[33]J. A. Campos-Gonzalez-Angulo and J. Yuen-Zhou, "Generalization of the tavis–cummings model for multi-level anharmonic systems: Insights on the second excitation manifold," The Journal of Chemical Physics **156** (2022).
[34]F. Herrera and F. C. Spano, "Absorption and photoluminescence in organic cavity qed," Phys. Rev. A: At. Mol. Opt. Phys. **95**, 053867 (2017).
[35]J. del Pino, J. Feist, and F. J. Garcia-Vidal, "Quantum theory of collective strong coupling of molecular vibrations with a microcavity mode," New Journal of Physics **17**, 053040 (2015).
[36]J. A. Campos-Gonzalez-Angulo, R. F. Ribeiro, and J. Yuen-Zhou, "Resonant catalysis of thermally activated chemical reactions with vibrational polaritons," Nature communications **10**, 4685 (2019).
[37]J. R. Mannouch and J. O. Richardson, "A partially linearized spin-mapping approach for simulating nonlinear optical spectra," The Journal of Chemical Physics **156** (2022).
[38]A. M. Branczyk, D. B. Turner, and G. D. Scholes, "Two-dimensional electronic spectroscopy for the quantum-optics enthusiast," arXiv preprint arXiv:1307.5855 (2013).
[39]A. M. Brańczyk, D. B. Turner, and G. D. Scholes, "Crossing disciplines - a view on two-dimensional optical spectroscopy," Annalen der Physik **526**, 31–49 (2014), https://onlinelibrary.wiley.com/doi/pdf/10.1002/andp.201300153.
[40]P. H. Lambrev, P. Akhtar, and H.-S. Tan, "Insights into the mechanisms and dynamics of energy transfer in plant light-harvesting complexes from two-dimensional electronic spectroscopy," Biochimica et Biophysica Acta (BBA)-Bioenergetics **1861**, 148050 (2020).
[41]S. Biswas, J. Kim, X. Zhang, and G. D. Scholes, "Coherent two-dimensional and broadband electronic spectroscopies," Chemical Reviews **122**, 4257–4321 (2022).
[42]K. Kwak, S. Park, I. J. Finkelstein, and M. D. Fayer, "Frequency-frequency correlation functions and apodization in two-dimensional infrared vibrational echo spectroscopy: A new approach," The Journal of Chemical Physics **127**, 124503 (2007), https://pubs.aip.org/aip/jcp/article-pdf/doi/10.1063/1.2772269/10925461/124503_1_online.pdf.
[43]A. O. Caldeira and A. J. Leggett, "Path integral approach to quantum brownian motion," Physica A: Statistical mechanics and its Applications **121**, 587–616 (1983).
[44]A. Nitzan, *Chemical dynamics in condensed phases: relaxation, transfer, and reactions in condensed molecular systems* (Oxford university press, 2024).